NJC

Accepted Manuscript

This is an *Accepted Manuscript*, which has been through the Royal Society of Chemistry peer review process and has been accepted for publication.

Accepted Manuscripts are published online shortly after acceptance, before technical editing, formatting and proof reading. Using this free service, authors can make their results available to the community, in citable form, before we publish the edited article. We will replace this *Accepted Manuscript* with the edited and formatted *Advance Article* as soon as it is available.

You can find more information about *Accepted Manuscripts* in the Information for Authors.

Please note that technical editing may introduce minor changes to the text and/or graphics, which may alter content. The journal's standard Terms & Conditions and the Ethical guidelines still apply. In no event shall the Royal Society of Chemistry be held responsible for any errors or omissions in this *Accepted Manuscript* or any consequences arising from the use of any information it contains.

ROYAL SOCIETY OF CHEMISTRY

www.rsc.org/njc

Colour Graphic:

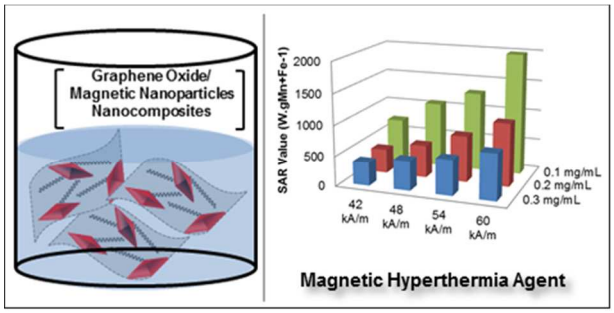

Description:

The SAR values of the magnetic nanocomposites increased by approximately two-fold when the concentration was reduced by a factor of 3.

New Journal of Chemistry Accepted Manuscript

New Journal of Chemistry

RSCPublishing

ARTICLE

Concentration-dependent Magnetic Hyperthermic Response of Manganese Ferrite-loaded Ultrasmall Graphene Oxide Nanocomposites

Cite this: DOI: 10.1039/x0xx00000x

Received 00th January 2012,
Accepted 00th January 2012

DOI: 10.1039/x0xx00000x

www.rsc.org/

Erwin Peng,[a] Jun Ding[a] and Jun Min Xue[a]

Water soluble and biocompatible ~18nm manganese-doped ferrite $(Mn_xFe_{1-x})Fe_2O_4$ decorated on ultrasmall graphene oxide (GO) nanocomposites were synthesized. The ultra-small nanocomposites with hydrodynamic size of 50.6 ± 0.3 nm and approximately ~80 nm/ ~20nm in its lateral dimension and thickness (from AFM analysis) indicated sheet-like structure with only few nanoparticles attached, were fabricated. Concentration-dependent magnetic hyperthermic response of such nanocomposites under alternating magnetic field (AMF) at very dilute condition (< 0.3mg.mL^{-1}) was investigated. The field-dependent specific absorption rate (SAR) values of the nanocomposites were found to have increased by approximately two-fold when their concentration was reduced by a factor of 3. Such nanocomposites also exhibited excellent colloidal stability as well as suitable biocompatibility up to 2 mM iron concentration with NIH/3T3 fibroblast cells.

Introduction

Ferrite-based magnetic nanoparticles (MFe_2O_4, where M = Fe, Mn, Co, Ni, Zn and etc) exhibited superparamagnetism properties below certain nanoparticle sizes range.[1] Because of this magnetic behaviour, such functional nanoparticles have been potentially exploited for various biomedical applications such as T_2 contrast agent for MRI, drug delivery as well as magnetic hyperthermia agents.[2] Of all different types of ferrite-based magnetic nanoparticles, manganese-doped ferrite $(Mn_xFe_{1-x})Fe_2O_4$, where x range from 0 to 1, is the most suitable candidate for the aforementioned applications due to its high magnetic susceptibility and high mass magnetization.[1]

Specifically for magnetic hyperthermia application, when superparamagnetic nanoparticles are exposed to an alternating magnetic field (AMF), both Neel and Brownian relaxation take place, due to the attempt to align the magnetic moment against the external magnetic field. Briefly, Neel relaxation is due to the rotation of magnetization vector while Brownian relaxation occurs due to the rotation of the nanoparticle itself.[2a] When dispersed in aqueous medium, such relaxation processes eventually results in a heat release to the surrounding environment. Because of this unique characteristic, superparamagnetic nanoparticles have been exploited as heating agent for (1) cancer therapy whereby localized heating to ~42^{o}C is required to induce thermal ablation of the cancer cell or (2) thermal-induced drug release for cancer therapeutics.[2d-e,3] Previously, various factors influencing the heating capacity of the magnetic nanoparticles, inclusive of size, shape, monodispersity (size distribution), morphology, composition as well as concentration, have been discussed in various literatures.[4] In practice, the *in-vivo* use of magnetic nanoparticles as hyperthermia agents requires a nanocomposite system which possess high heating capacity, to achieve high SAR values and shorter heating time, even at very low dosage (low concentration). With regards to such conditions, various reported hyperthermic response and their SAR values measurement of magnetic nanoparticle at relatively high concentration (more than 1mg.mL^{-1}) are unsuitable.[4a,5] When such heating agent was injected intratumorally or intravenously during *in-vivo* and incubated with cancerous cells during *in-vitro* experiment, dilution occurred and the reported SAR values at the injection dose is over-estimated.[3a]

In the present work, a water-dispersible magnetic nanocomposites system based on graphene oxide (GO) materials was investigated to elucidate the hyperthermic response, especially at low concentration. As shown in **Scheme 1**, clusters of magnetic nanoparticles decorated on ultra-small GO nanosheets (denoted as MNCs) was synthesized, eliminating the need of any additional organic (*e.g.* polymeric coatings) and inorganic (*e.g.* silica or gold) coatings.[6] Graphene oxide was chosen as the host for the magnetic nanoparticles due to its excellent thermal conductivity in aqueous solvent.[7] As the heating efficiency of superparamagnetic nanoparticles increased when the magnetic properties increased, relatively large ~18nm manganese-doped ferrite nanoparticles $(Mn_xFe_{1-x})Fe_2O_4$ (denoted as MNPs) obtained from the typical thermal decomposition synthesis was employed.[8] Relying on the amphiphilicity of the GO and the reported interaction with oleylamine binder, hydrophobic MNPs can be water solubilized.[9] The synthesis process was adopted, with slight modification to keep the clusters size of magnetic nanoparticles

New Journal of Chemistry Accepted Manuscript

on the GO sheets minimal.[6a] Although the idea of decorating magnetic nanoparticles (*e.g.* magnetite) on GO sheets was not new, some of the existing protocols may experience colloidal instability problem due to the use of large GO sheet.[10] Therefore the formation of MNCs using the proposed method was more advantageous in terms of colloidal stability.

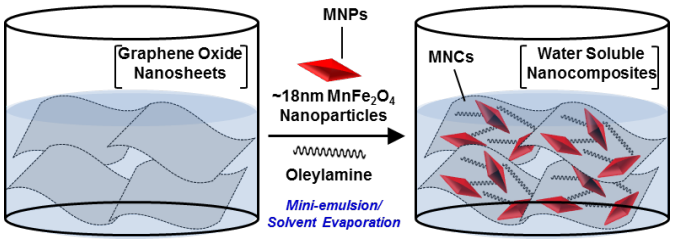

Scheme 1. Formation of manganese-doped ferrite nanoparticles-loaded ultrasmall graphene oxide nanocomposites (MNCs) through a simple mini-emulsion/solvent evaporation process.

Experimental Section

Materials

Manganese (II) acetylacetonate ($Mn(acac)_2$), iron (III) acetylacetonate ($Fe(acac)_3$; 97%), oleic acid (≥99%), benzyl ether (99%), oleylamine (70%) were purchased from Sigma-Aldrich Singapore. Chloroform and hexane (≥99.9%) were purchased from Fisher Scientific and used as-received.

Synthesis of ~18nm $(Mn_xFe_{1-x})Fe_2O_4$ Nanoparticles (MNPs)

Superparamagnetic MNPs with average size of ~18nm was simply synthesized through classical thermal decomposition reaction of acetylacetonate precursors in the presence of hydrophobic capping agent oleic acid and high-boiling point solvent benzyl ether (*b.p.*300°C).[8] Typically, 10 mmol Fe(acac)3, 5 mmol Mn(acac)2, 28 mmol of oleic acid and 35 mL of benzyl ether were charged into 100 mL three-neck round bottom flask. The resulting mixture was then heated up to 165°C under nitrogen gas flow protection and hold isothermally for 30 minutes. Subsequently, the mixture was further heated up to 280°C and maintained at this temperature for 30 minutes. The mixture was allowed to cool down and MNPs were precipitated by the addition of ethanol and isolated by using centrifugation, followed by subsequent re-dispersion into $CHCl_3$. Such washing procedures was repeated at least 3 times and MNPs was stored in $CHCl_3$ in a sealed glass vial at temperature 4°C.

Synthesis of ~18nm MNPs/ultrasmall GO Nanocomposites (MNCs)

To obtain water soluble MNPs, we firstly synthesized GO through classical Hummer's method.[11] The resulting dried powder of GO was mixed with oleylamine/$CHCl_3$ mixture and subseqeuently homogenized for 30 minutes. Subsequently, 3 mL of this GO/oleylamine in $CHCl_3$ mixture (approximately 4 $mg.mL^{-1}$ GO) was then mixed with 0.6 mL of MNPs in $CHCl_3$ (50 $mg.mL^{-1}$) and 36 mL of deionized water. The overall mixture was then homogenized by using ultrasonic homogenizer for 1 hour and transferred to a pre-heated beaker at 70°C. The $CHCl_3$ was simply evaporated away for 30 minutes in order to obtain MNPs decorated on GO nanocomposites (MNCs). Large contaminants were removed simply by centrifuging the MNCs at 10000 rpm for 10 minutes. The supernatant was collected and stored at room temperature.

Magnetic Hyperthermia Measurement

The magnetic hyperthermia measurement was simply conducted by exposing 1mL of MNCs sample in 15 mL centrifuge tube to external magnetic field (AMF) by using RF generator (Easyheat-5060, 4.2–10 kW, Ameritherm). The diameter of the induction coil was 0.034m. Optical fibre-based temperature probe (FluoTemp Series FTP-LN_2) was used to measure the sample temperature. The specific absorption rate (SAR) value of MNCs were simply calculated from the obtained AMF exposure time-dependent calorimetric measurement (Amplitude: 42–60 $kA.m^{-1}$; frequency 240 kHz; total exposure time of 900 seconds), following the equation:

$$\mathbf{SAR = C_{water}\ x\ (dT/dt)\ /\ (m_{Fe} + m_{Mn})}$$

where C_{water} is the specific heat of the medium, equal to 4.18 $Jg^{-1}{}^{o}C^{-1}$ for water. (dT/dt) is the initial slope of the time-dependent temperature curve (from the first 100 data points). (m_{Fe} + m_{Mn}) is the overall weight fraction of the magnetic element (both iron and manganese contributions were taken into account when calculating SAR value). For convenience, three different concentrations of MNCs sample were indicated as 0.1, 0.2 and 0.3 mg $Fe.mL^{-1}$ (equivalent to 0.14, 0.29 and 0.43 mg $MNPs.mL^{-1}$). (the error on SAR value was estimated by calculating the standard deviation of the SAR values obtained from the first 50, 100 and 200 data points).

In-vitro Cellular Cytotoxicity Measurement

The cell cytotoxicity of MNCs was determined from the in-vitro CCK-8 cytotoxicity assay using NIH/3T3 cells. NIH/3T3 cells were grown in DMEM (Dulbecco's Modified Eagle Medium) growth medium, supplemented with 10% bovine calf serum (BCS) at 37°C. 0.1 mL of NIH/3T3 cells (7500 cells/well) were seeded onto 96-well plate (TPP) for 12 hours and further incubated for 24 hours with 20 µL solutions containing various iron concentration of MNCs (0.01 mM to 2.0 mM Fe). Subsequently, 10 µL solution of CCK-8 was added and further incubated for 4 hours. The absorbance readings at 450nm (corresponds to the presence of live cells) were recorded using FluoStar Optima microplate reader.

Materials Characterization

The magnetic properties of MNPs and MNCs were characterized by vibrating sample magnetometer (VSM; Lakeshore Model 7407) at room temperature (~298K). The x-ray diffraction pattern of MNPs and MNCs were obtained from the powder diffractometer (Bruker D8 Advance Diffractometer System) with Cu Kα source (λ = 1.5418Å). The transmission electron microscopy (TEM) image of MNPs and MNCs were obtained by using JEOL-3010F TEM (accelerating voltage of 300kV). The average hydrodynamic diameters of MNCs were recorded on Malvern Zetasizer Nano-ZS. The thermogravimetric analysis (TGA) was done on dried MNCs sample using New Castle SDTQ600. The iron concentration of MNCs was determined form the inductively coupled plasma-optical emission spectroscopy (ICP-OES) analysis (Perkin-Elmer Dualview Optima 5300 DV ICP-OES System).

New Journal of Chemistry Accepted Manuscript

This journal is © The Royal Society of Chemistry 2012

Result and Discussion

Ultrasmall GO nanosheets

As shown in **Fig.1**, the AFM image indicated that ultra-small GO were successfully fabricated. The average size of the as-synthesized GO, from the chemical synthetic route coupled with extension homogenization process by using probe sonication, was less than 100 nm. The cross section analysis of the ultra-small GO indicated a thickness around 1.03 nm which was equivalent to mono-layer of GO sheet.[12] The lateral dimension from the high magnification AFM image was no more than 100 nm.

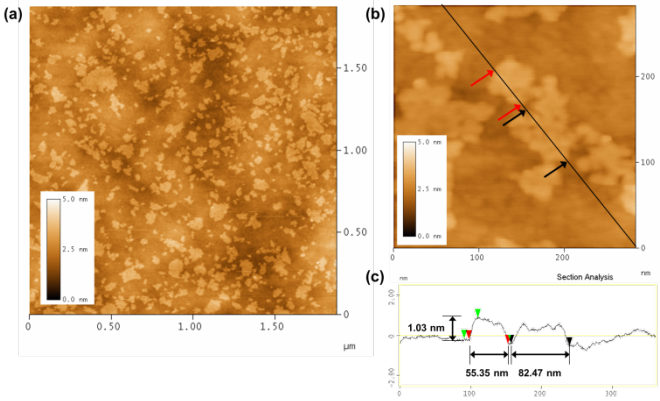

Fig. 1 (a) Low magnification and (b) high magnification AFM image of GO with (c) the GO cross section analysis.

Synthesis of MNPs and MNCs

Hydrophobic manganese-doped ferrite nanoparticles were synthesized through the classical high temperature thermolysis of mixed-metal acetylacetonate precursors. The TEM image of the as-synthesized MNPs was given in **Fig.2a**. Octahedrally-shaped nanoparticles dispersed in $CHCl_3$ were obtained. The hydrophobic MNPs were then water-solubilized using ultra-small GO sheets that have been pre-modified with oleylamine, forming the water soluble magnetic nanocomposite (MNCs). In this case, oleylamine acted as an intermediate binder that promoted the hydrophobic–hydrophobic interaction between ultra-small GO sheets and the hydrophobic MNPs. The amount of oleylamine used here was only sufficient to dissolve the grapheme oxide as excess oleylamine was washed off by centrifugation prior to the nanocomposite formation. (see **Fig.S1** for the illustration) The MNPs were successfully water-solubilized and the TEM image of MNCs in **Fig.2b** demonstrated that the MNPs were decorated on the surface of GO sheets without any apparent size and morphology change.

From the XRD patterns presented in **Fig.2c**, the peaks position and their relative intensities before and after the formation of MNCs were identical. Both patterns highlighted identical peaks at 2θ range = 20–65° which matched the (220), (311), (400), (422), (333) and (440) planes of the Jacobsite crystal structure ($MnFe_2O_4$; JCPDS 74-2403). Overall, the XRD analysis indicated the water solubilisation process had negligible effect on the MNPs crystallinity. The high resolution TEM (HRTEM) images of highly crystalline MNPs and MNCs (insets of **Fig.2a,b**) showed lattice fringes with separation distance of 0.492 and 0.296 nm which matched well with (111) and (220) lattice planes *d*-spacing of Jacobsite structure. The identical diffraction rings from the SAED patterns for MNPs and MNCs were indexed correspondingly to (220), (311), (331), (422), (333) and (440) indices of Jacobsite.

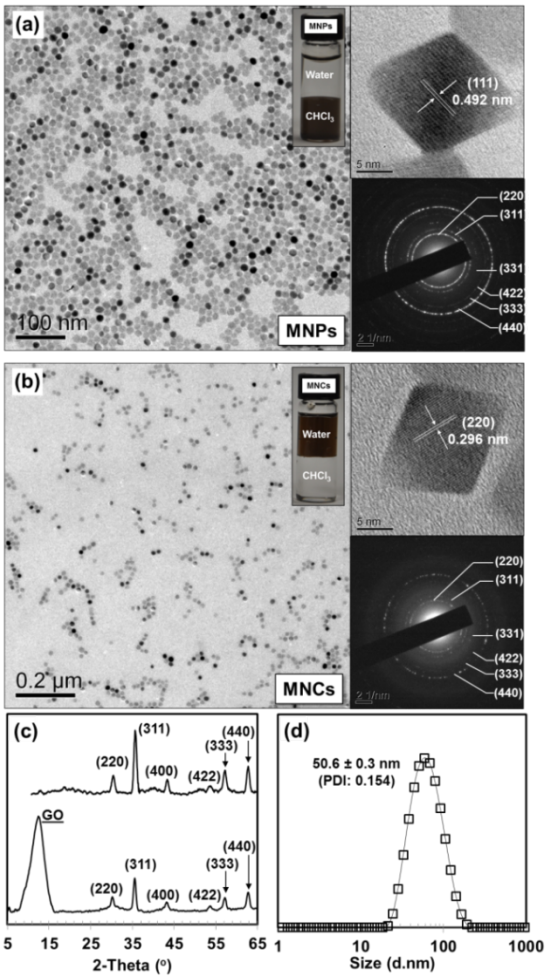

Fig. 2 TEM images of (a) as-synthesized MNPs dispersed in $CHCl_3$ and (b) MNCs dispersed in water. (c) XRD patterns of MNPs and MNCs. (d) Hydrodynamic size distribution of MNCs in water.

The TEM size distribution histograms in **Fig.3** showed the average size of MNPs in $CHCl_3$ and after formation of MNCs (after prolonged sonication to be 18.8 ± 2.2 nm and 18.5 ± 2.9 nm. These average sizes were quite close and consistent which implied that the formation of the nanocomposites through the extended sonication has no significant effect towards the average MNPs size. From the XRD patterns, the average crystallite sizes of MNPs before and after MNCs formation were calculated using Scherrer equation using the most intense (311) XRD peak FWHM. The calculated crystallite size of 18.14 nm and 18.55 nm, for MNPs and MNCs respectively, were in a good agreement with the average size of MNPs and MNCs measured from TEM analysis. Despite the successful formation of MNCs, the presence of GO sheets was not detected from TEM analysis, even at higher magnification (**Fig.S2a**). The presence of GO sheets however, was confirmed through the XRD pattern (see **Fig.2c**) in which the XRD peak at around 2θ of ~12.4° corresponded to the presence of GO sheets.

New Journal of Chemistry Accepted Manuscript

Such peak was due to 0.71 nm (001) planes spacing between GO sheets.[13]

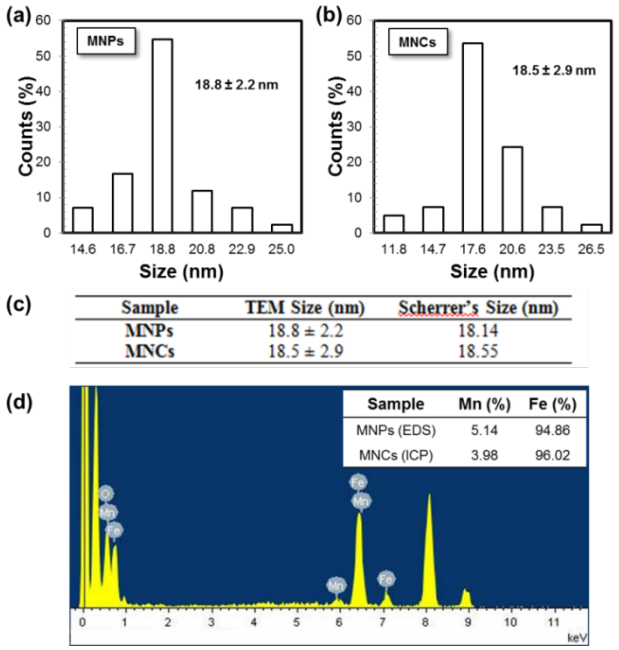

Fig. 3 Size distribution histograms of MNPs: (a) as-synthesized and (b) after formation of MNCs. (c) Summary of TEM size and calculated Scherrer size. (d) EDS spectrum of MNPs.

From **Fig.3**, the determination of Fe/Mn ratio was accomplished by EDS analysis of MNPs and ICPs analysis of MNCs. The EDS of MNPs revealed Fe/Mn ratio of 18.46. Meanwhile the ICPs analysis of MNCs reported Fe/Mn ratio of 24.13. Both results opposed the ideal Fe/Mn ratio of 2 (the precursors ratio), therefore suggesting the formation of $(Mn_xFe_{1-x})Fe_2O_4$ structure with x in the range of 0.04 - 0.05. The XRD analysis of the diffraction peaks also showed that the calculated average lattice parameter of *a* of the MNPs were estimated to be around 8.43Å. This value was between the average lattice parameter of $MnFe_2O_4$ (JCPDS 74-2403; a = 8.51Å) and $(Mn_0Fe_1)Fe_2O_4$ (JCPDS 65-3107; a = 8.39Å).[14]

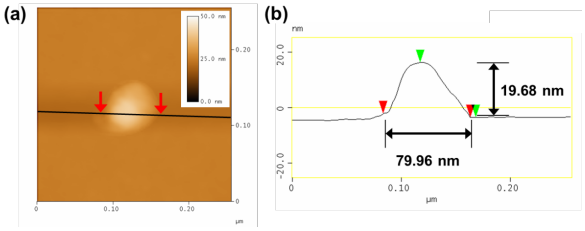

Fig. 4 (a) High magnification AFM image of single MNCs spin-coated onto Si-substrate. (b) Cross section profile of single MNCs.

As depicted in **Fig.4**, the high magnification AFM image of MNCs and its cross-section analysis of single MNCs showed a lateral dimension of about ~80nm and approximately ~20 nm in its thickness. Considering the original ~18nm MNPs core size (from TEM and Scherrer formula), the as-measured hydrodynamic size of MNCs (50.6 ± 0.3 nm) when dispersed in water indicated that MNCs comprised of a mild aggregation of several MNPs on the surface of ultra-small GO sheets. The additional 1-2 nm difference in the MNCs thickness from the MNPs average size, was clearly ascribed to the presence of mono- or double-layer of ultra-small GO sheets (with oleylamine binder). In order to visually observe the morphology of MNCs, a further experiment to enhance the MNCs contrast was done by tagging MNCs with higher molecular weight polymer such mPEG-NH_2 (MW 5000) using carbodiimide chemistry, EDC/NHS reagent. From **Fig.S2b**, the high magnification TEM image of MNCs-tagged with PEG showed a slight contrast enhancement which indicated the presence of the sheet-like structure. From the image, the lateral size matched very well with the AFM analysis and MNPs were observed to be decorated on the surface of ultrasmall GO sheet. The measured zeta potential of MNCs from DLS experiment revealed a positively charged surface of 44.9 ± 1.2 mV. The positive zeta potential value was beneficial to provide electrostatic repulsion to stabilized MNCs in aqueous solvent. The positive surface charge was due the presence of the positively charged amine functional group ($-NH_3^+$).[6]

The magnetic properties of MNPs and MNCs were analysed by using vibrating sample magnetometer (VSM) at room temperature (~298K). The saturation magnetization (M_S) values for MNPs and MNCs were 96.9 emu.g^{-1} and 24.8 emu.g^{-1} as given in the hysteresis loop in **Fig.5a**. The drastic decrease in the M_S value of approximately ~74.4% was attributed to the presence of approximately ~75.7% organic moieties as determined from the thermogravimetric analysis (TGA) results in **Fig.5b**. Overall, the as-synthesized magnetic nanocomposites MNCs still exhibited superparamagnetism with almost negligible remnant magnetization (M_R) and coercive field (H_C) (as observed from the hysteresis loop near zero-field given in **Fig.S3**). Such behaviour was beneficial to prevent the magnetic aggregations between MNCs without the presence of magnetic field.

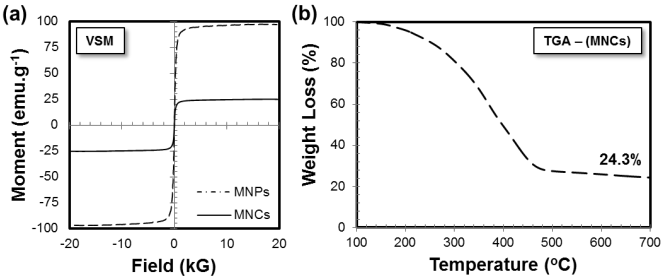

Fig. 5 (a) As-measured hysteresis loops of MNPs and MNCs (dried samples) at room temperature (~298K). (b) Heating profile of MNCs samples from the thermogravimetric analysis (TGA) experiment.

Magnetic Hyperthermic Response: Oleylamine-modified GO

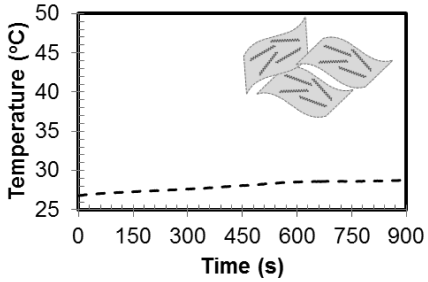

Fig. 6 Time-dependent temperature curve of oleylamine-modified GO in water (AMF 60 kA.m^{-1}; AC field at 240 kHz frequency)

In a separate preliminary experiment, **Fig.6** depicted the time-dependent magnetic hyperthermic response of 1 mL pure oleylamine-modified GO dispersed in water. The concentration

New Journal of Chemistry Accepted Manuscript

This journal is © The Royal Society of Chemistry 2012

of pure oleylamine-modified GO was more or less equivalent to the MNCs sample. When exposed to very high AMF at 60 kA.m^{-1}, the overall oleylamine-modified GO solution was increased by approximately 1.5–2.0^{o}C after 900 seconds of heating. This non-specific temperature rise was due to the induced Eddy currents (inevitable loses) which subsequently generate heats release to the local surrounding.

Magnetic Hyperthermic Response: Core Size Effect

To obtain an effective heating efficiency, larger core size nanoparticles (closer to the limit of the superparamagnetic single domain size limit) was preferred in order to maximize the specific adsorption rate (SAR) value. This was because the nanoparticles' surface spin canting decreased as size decrease before reaching the single domain size limit which resulted in the improvement of magnetic properties. Beyond this critical size, single domain nanoparticles turn into multidomain state, and therefore the heat dissipation reduced significantly.[4h]

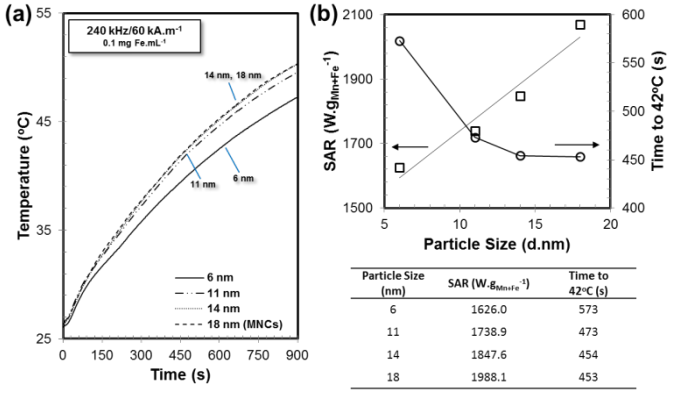

Particle Size (nm)	SAR (W.g$_{Mn+Fe}$ $^{-1}$)	Time to 42°C (s)
6	1626.0	573
11	1738.9	473
14	1847.6	454
18	1988.1	453

Fig. 7 (a) Time-dependent temperature curve of MNCs samples with various MNPs core size, dispersed in water under exposure of AMF 60 kA.m^{-1}; AC field at 240 kHz frequency (0.1 mg Fe.mL^{-1}). (b) Plot of SAR values and the heating time required for reaching 42^{o}C against the MNPs core sizes.

Fig.7 summarized the SAR values for MNCs and the time required to reach 42^{o}C for various core sizes, approximately 6nm, 11nm, 14nm and 18nm (60 kA.m^{-1} AMF amplitude; 240 kHz frequency; 0.1 mg Fe.mL^{-1}). The average MNCs hydrodynamic size was around 50–55nm with SAR values of 1626.1 W.g$_{(Mn+Fe)}^{-1}$ for 6nm MNPs, 1738.9 W.g$_{(Mn+Fe)}^{-1}$ for 11nm MNPs, 1847.6 W.g$_{(Mn+Fe)}^{-1}$ for 14nm MNPs and 1988.1 W.g$_{(Mn+Fe)}^{-1}$ for 18nm MNPs. The comparison of the SAR values of MNCs formed with these four different superparamagnetic core sizes (below the single domain critical size) emphasized the trend of increasing of SAR values as the core size increased. From **Fig.S4**, when oleylamine-modified GO was compared against simple amphiphilic polymer encapsulation to obtain water-dispersible MNPs, it was observed that the heating efficiency of MNCs sample at 0.1 mg Fe.mL^{-1} was much higher than the polymer-coated MNPs samples at 0.3 mg Fe.mL^{-1}. These results clearly demonstrated that the use of GO sheets actually allowed faster MNPs relaxation as compared to the typical polymer coating. When polymer coating was used, the presence of "encapsulation" coating acted as heat barrier which slowed down the heat release to the environment.

When compared with the 80–90nm cluster size MNCs from literatures, the SAR value of MNCs formed with 6nm (1541.6 W.g$_{(Mn+Fe)}^{-1}$), 11nm (1231.7 W.g$_{(Mn+Fe)}^{-1}$) and 14nm (1586.8 W.g$_{(Mn+Fe)}^{-1}$) were lower than the 50–55 nm cluster size MNCs presented in **Fig.7**.[6a] The reduction in the cluster size to smaller nanocomposites reduced the number of MNPs embedded onto GO. Hence, the inter-MNPs particles interaction within the same GO sheet was minimized. Small clusters size magnetic nanocomposite was also preferred because it can dissipate heat more effectively, allowing higher hyperthermic response while maintaining the overall colloidal stability. From the comparison, MNCs formed with ~18nm MNPs (as characterized in **Fig.2**) was selected to be further investigated.

Magnetic Hyperthermic Response: Concentration Effect

The concentration-effect towards the hyperthermic response of water soluble MNCs (with ~18 MNPs core) samples at various iron concentration (0.1, 0.2 and 0.3 mg Fe.mL^{-1}) were investigated under various AMF at 240 kHz frequency with magnitude range of 42–60 kA.m^{-1}. Although the AMF amplitude (H) and the frequency (f) exceeded the physiological limit (the Brezovich criterion, where $H.f$ should be below 5 x 10^{9} A.m^{-1}s^{-1}), such limit can be relaxed by nine-times ($H.f$ < 4.5 x 10^{10} A.m^{-1}s^{-1}) due to the difference in the coil diameter used in the experiment (see **Table S1** in ESI for further details). The AMF exposure time-dependent temperature curve of the MNCs sample at various concentrations presented in **Fig.8a-c** showed very responsive hyperthermic responses due to high magnetic susceptibility of MNCs. It was observed that the rate of temperature increment systematically increased with the increase in the overall magnetic nanoparticles concentrations.

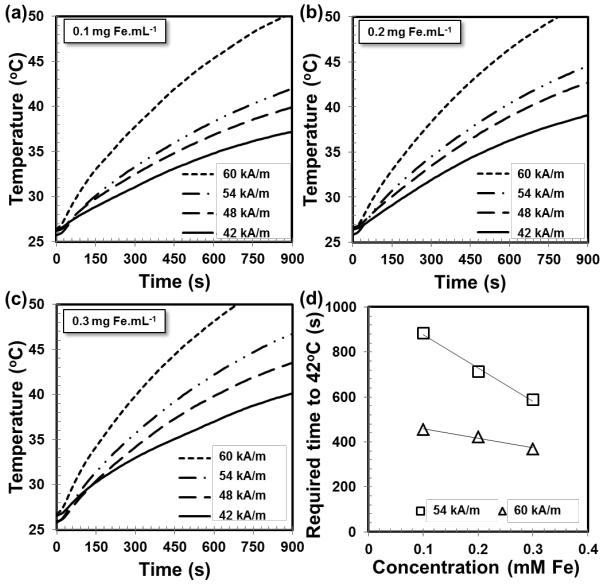

Fig. 8 Time-dependent temperature curve of MNCs samples (~18nm core MNPs) at various iron concentrations: (a) 0.1 mg Fe.mL^{-1}, (b) 0.2 mg Fe.mL^{-1} and (c) 0.3 mg Fe.mL^{-1}. (d) Concentration-dependent required time for reaching 42^{o}C for MNCs sample.

From **Fig.8d**, the time required for MNPs to reach 42^{o}C with 54.05 kA.m^{-1} field from room temperature was 885s, 714s and 588s for 0.1, 0.2 and 0.3 mg Fe.mL^{-1} MNCs respectively. Meanwhile at higher field of 60 kA.m^{-1}, 455s, 423s and 370s were required for 0.1, 0.2 and 0.3 mg Fe.mL-1 MNCs, almost half of the time required at 54.05 kA.m^{-1}. At lower fields of 42 kA.m^{-1} and 48 kA.m^{-1}, all three concentrations of MNCs could

New Journal of Chemistry Accepted Manuscript

not reach 42°C within 900 seconds of heating time. From the field-dependent SAR values plot in **Fig.8**, the heating efficiency of MNCs, represented by SAR value, increased with AMF as predicted.[4,5] The SAR values of MNCs also decreased significantly with the increase of the MNCs concentration. And overall, increasing the concentration from 0.1 mg Fe.mL^{-1} by 2- or 3-times did not reduce the heating time required to reach 42°C proportionally. These results suggested that internal interactions occurred between the MNCs which hindered the effective heat dissipation during relaxation.

Considering a hypothetical model whereby the oleic-acid coated MNPs were directly decorated on GO, the absence of high molecular weight organic/inorganic coating (*e.g.* amphiphilic polymer or silica) allowed a close interaction between the decorated MNPs and the surroundings. In such configuration, the separation distance between MNCs played a critical role as it determines the resultant MNCs dipole–dipole interactions (see illustration given in **Fig.S6**). Thus, the increase in MNCs concentration was associated with the increase in dipolar interactions which stabilized the MNCs collectively against re-orientation towards the applied field.[15a,b] Due to its nature; Brownian relaxation was less-dependent on the heating agent concentration and the aforementioned dipolar interactions. However, stronger dipolar interaction prolonged Neel relaxation, while weak dipolar interactions promoted faster Neel relaxation.[15c]

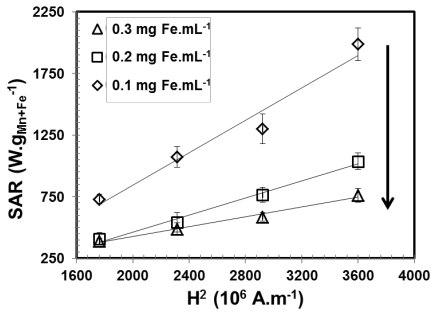

Fig. 9 Field-dependent SAR values of MNCs at various concentrations.

Because of the dipolar interaction, when the MNCs concentration increase, it became more prominent in **Fig.9** that the SAR value became less dependent on the field due to slower Neel relaxation. As MNCs was exposed to high frequency AMF (more than 100 kHz), Neel relaxation dominated the heat/energy dissipation mechanism as compared to Brownian relaxation. Therefore, when the separation distance between MNCs nanocomposites decreased due to increased concentration, Neel relaxation was prolonged. Because of this, the overall decrease in the effective mass-heating efficiency trend shown in **Fig. 9** can be explained.[4h,15c-d] The concentration effect on SAR values was more prominent at lower field than at higher field amplitude. Due to this, at lower field of 42 kA.m^{-1}, the SAR value of 0.3 mg Fe.mL^{-1} MNCs differ by only 5% as compared to the SAR value of 0.2 mg Fe.mL^{-1}. While at higher field of 60 kA.m^{-1}, the SAR value of 0.3 mg Fe.mL^{-1} MNCs differ by approximately 25% as compared to the SAR value of 0.2 mg Fe.mL^{-1}. At higher AMF, the energy input to the system from the AMF generator was sufficient to overcome the energy barrier for the relaxation mechanism.

From our experimental results, it can be concluded that high SAR value of 1988.1 $Wg_{(Mn+Fe)}^{-1}$ was achieved at 60 kA.m^{-1} field with concentration as low as 0.1 mg Fe.mL^{-1} (0.14 mg ferrites per mL).

In-vitro Cell Cytotoxicity and Colloidal Stability

In various in-vitro applications especially during hyperthermic application, the nanocomposites should neither disintegrate nor aggregate. For such reason, temperature-dependent stability test of MNCs in the temperature range of 24°C to 48°C were assessed by using DLS experiment. The plot of MNCs hydrodynamic size against temperature given in **Fig.10a** indicated that MNCs sample was stable in the aforementioned temperature range without any observable aggregation.

From the cytotoxicity assays using cell counting kit-8 (CCK-8) presented in **Fig.10b**, NIH/3T3 fibroblast cells were more than 95% viable after 24 hours incubation with MNCs at various concentration (0.01–2.0 mM Fe). Thus, MNCs nanocomposite loaded with ~18nm MNPs can be considered to be biocompatible with NIH/3T3 fibroblast cells up to 2 mM iron concentration (approximately ~0.11 mg Fe.mL^{-1}). Based on the dilution sequences of the starting materials, 2 mM iron concentration (160 μg Fe.mL^{-1}), approximately equal to 300 μg.mL^{-1} nanoparticles. This was equivalent to at least 40 μg.mL^{-1} GO sheets. Hence the cell viability given in **Fig.10b** also indicated that GO sheets were compatible with NIH/3T3 fibroblast cells up from 0.2 μg.mL^{-1} to 40 μg.mL^{-1}. Such good biocompatibility has also been reportedly previously for ultrasmall GO sheets, as well as the typical GO sheets obtained from Hummer's method.[16]

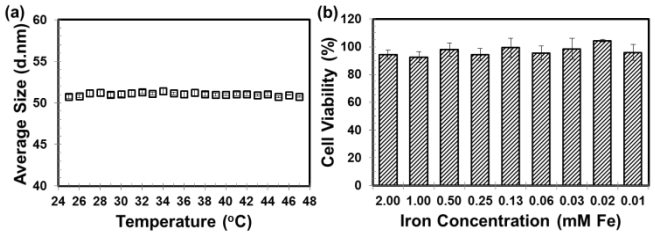

Fig. 10 Temperature-dependent stability test of MNCs (24°C–48°C). (b) NIH/3T3 cell viability of MNCs incubated for 24 hours at 37°C.

Moreover, a further time-dependent stability test indicated that MNCs sample exhibited excellent colloidal stability in water at 37°C for more than 90 hours without any increase in the hydrodynamic size (see ESI **Fig.S7**). The overall hydrodynamic size over 90 hours was calculated to be 51.0 ± 0.2 nm. Both the colloidal stability and cytotoxicity test results favoured MNCs to be used for biomedical applications, especially magnetic hyperthermia.

Conclusions

In conclusion, water-soluble nanocomposites consisting of superparamagnetic ~18nm manganese-doped ferrite nanoparticles $(Mn_xFe_{1-x})Fe_2O_4$ decorated on ultra-small GO nanosheet (host) have been successfully synthesized. Using this system, the concentration-effect on the AMF hyperthermic effect at very dilute condition was studied. It was observed that the SAR values of MNCs increased by two-fold as the nanoparticles concentration was lowered by a factor of 3. Lastly

New Journal of Chemistry Accepted Manuscript

 This journal is © The Royal Society of Chemistry 2012

MNCs were found to have good colloidal stability with low cytotoxicity effect to NIH/3T3 cells below 2 mM iron concentration.

Acknowledgements

This work is financially supported by MOE's Singapore FRC Grant WBS R-284-000-102-112. The author would like to thank Department of Materials Science and Engineering, National University of Singapore for the current on-going research scholarship funding.

Notes and references

[a] Department of Materials Science and Engineering, Faculty of Engineering. National University of Singapore, 9 Engineering Drive 1, Singapore 117576. E-mail: msexuejm@nus.edu.sg; Fax: +65 6776 3604; Tel: +65 6516 4655.

† Electronic Supplementary Information (ESI) available: [details of any supplementary information available should be included here]. See DOI: 10.1039/b000000x/

1 (a) J.-H. Lee, Y.-M. Huh, Y.-w. Jun, J.-w. Seo, J.-t. Jang, H.-T. Song, S. Kim, E.-J. Cho, H.-G. Yoon, J.-S. Suh and J. Cheon, *Nat Med*, 2007, **13**, 95-99; (b) J. Mohapatra, A. Mitra, D. Bahadur and M. Aslam, *CrystEngComm*, 2013, **15**, 524-532; (c) S. Sun, H. Zeng, D. B. Robinson, S. Raoux, P. M. Rice, S. X. Wang and G. Li, *J. Am. Chem. Soc.*, 2003, **126**, 273-279; (d) J.-t. Jang, H. Nah, J.-H. Lee, S. H. Moon, M. G. Kim and J. Cheon, *Angew. Chem. Int. Ed.*, 2009, **48**, 1234-1238.

2 (a) D. Yoo, J.-H. Lee, T.-H. Shin and J. Cheon, *Acc. Chem. Res.*, 2011, **44**, 863-874; (b) S. Brulé, M. Levy, C. Wilhelm, D. Letourneur, F. Gazeau, C. Ménager and C. Le Visage, *Adv. Mater.*, 2011, **23**, 787-790; (c) V. Sokolova and M. Epple, *Angew. Chem. Int. Ed.*, 2008, **47**, 1382-1395; (d) N. Lee, Y. Choi, Y. Lee, M. Park, W. K. Moon, S. H. Choi and T. Hyeon, *Nano Lett.*, 2012, **12**, 3127-3131; (e) P. Guardia, R. Di Corato, L. Lartigue, C. Wilhelm, A. Espinosa, M. Garcia-Hernandez, F. Gazeau, L. Manna and T. Pellegrino, *ACS Nano*, 2012, **6**, 3080-3091.

3 (a) B. Thiesen and A. Jordan, *Int. J. Hyperthermia*, 2008, **24**, 467-474; (b) K. H. Bae, M. Park, M. J. Do, N. Lee, J. H. Ryu, G. W. Kim, C. Kim, T. G. Park and T. Hyeon, *ACS Nano*, 2012, **6**, 5266-5273; (c) M. Creixell, A. C. Bohórquez, M. Torres-Lugo and C. Rinaldi, *ACS Nano*, 2011, **5**, 7124-7129; (d) J.-P. Fortin, F. Gazeau and C. Wilhelm, *Eur Biophys J*, 2008, **37**, 223-228; (e) A. Chalkidou, K. Simeonidis, M. Angelakeris, T. Samaras, C. Martinez-Boubeta, L. Balcells, K. Papazisis, C. Dendrinou-Samara and O. Kalogirou, *J. Magn. Magn. Mater.*, 2011, **323**, 775-780; (f) H. Oliveira, E. Pérez-Andrés, J. Thevenot, O. Sandre, E. Berra and S. Lecommandoux, *J. Control. Release*, 2013, **169**, 165-170.

4 (a) J.-H. Lee, J.-t. Jang, J.-s. Choi, S. H. Moon, S.-h. Noh, J.-w. Kim, J.-G. Kim, I.-S. Kim, K. I. Park and J. Cheon, *Nat Nano*, 2011, **6**, 418-422; (b) B. Mehdaoui, A. Meffre, J. Carrey, S. Lachaize, L.-M. Lacroix, M. Gougeon, B. Chaudret and M. Respaud, *Adv. Funct. Mater.*, 2011, **21**, 4573-4581; (c) H. Rudolf, D. Silvio and R. Michael, *J. Phys: Condens. Matt.*, 2008, **20**, 385214; (d) H. M. Joshi, Y. P. Lin, M. Aslam, P. V. Prasad, E. A. Schultz-Sikma, R. Edelman, T. Meade and V. P. Dravid, *J. Phys. Chem. C*, 2009, **113**, 17761-17767; (e) A. Urtizberea, E. Natividad, A. Arizaga, M. Castro and A. Mediano, *J. Phys. Chem. C*, 2010, **114**, 4916-4922; (f) D. Serantes, D. Baldomir, C. Martinez-Boubeta, K. Simeonidis, M. Angelakeris, E. Natividad, M. Castro, A. Mediano, D. X. Chen, A. Sanchez, L. I. Balcells and B. Martinez, *J. Appl. Phys.*, 2010, **108**, 073918-073915; (g) P. Hugounenq, M. Levy, D. Alloyeau, L. Lartigue, E. Dubois, V. Cabuil, C. Ricolleau, S. Roux, C. Wilhelm, F. Gazeau and R. Bazzi, *J. Phys. Chem. C*, 2012, **116**, 15702-15712; (h) K. D. Bakoglidis, K. Simeonidis, D. Sakellari, G. Stefanou and M. Angelakeris, *Magn, IEEE Trans.*, 2012, **48**, 1320-1323; (i) P. de la Presa, Y. Luengo, M. Multigner, R. Costo, M. P. Morales, G. Rivero and A. Hernando, *j. Phys. Chem. C*, 2012, **116**, 25602-25610; (j) J.-P. Fortin, C. Wilhelm, J. Servais, C. Ménager, J.-C. Bacri and F. Gazeau, *J. Am. Chem. Soc.*, 2007, **129**, 2628-2635.

5 (a) X. L. Liu, H. M. Fan, J. B. Yi, Y. Yang, E. S. G. Choo, J. M. Xue, D. D. Fan and J. Ding, *J. Mater. Chem.*, 2012, **22**, 8235-8244; (b) D. Maity, P. Chandrasekharan, C.-T. Yang, K.-H. Chuang, B. Shuter, J.-M. Xue, J. Ding and S.-S. Feng, *Nanomedicine*, 2010, **5**, 1571-1584; (c) L.-Z. Bai, D.-L. Zhao, Y. Xu, J.-M. Zhang, Y.-L. Gao, L.-Y. Zhao and J.-T. Tang, *Mater. Lett.*, 2012, **68**, 399-401.

6 (a) E. Peng, E. S. G. Choo, P. Chandrasekharan, C.-T. Yang, J. Ding, K.-H. Chuang and J. M. Xue, *Small*, 2012, **8**, 3620-3630; (b) Y. Sheng, X. Tang, E. Peng and J. Xue, *J. Mater. Chem. B*, 2013, **1**, 512-521.

7 Y. Wei, X. Huaqing and B. Dan, *Nanotechnology*, 2010, **21**, 055705.

8 (a) L. Li, Y. Yang, J. Ding and J. Xue, *Chem. Mater.*, 2010, **22**, 3183-3191; (b) E. S. G. Choo, E. Peng, R. Rajendran, P. Chandrasekharan, C.-T. Yang, J. Ding, K.-H. Chuang and J. Xue, *Adv. Funct. Mater.*, 2013, **23**, 496-505.

9 (a) J. Kim, L. J. Cote, F. Kim, W. Yuan, K. R. Shull and J. Huang, *J. Am. Chem. Soc.*, 2010, **132**, 8180-8186; (b) D. W.-P. Pang, F.-W. Yuan, Y.-C. Chang, G.-A. Li and H.-Y. Tuan, *Nanoscale*, 2012, **4**, 4562-4570; (c) W. Yu, H. Xie, X. Wang and X. Wang, *Nanoscale Res. Lett.*, 2011, **6**, 47..

10 (a) Y. Zhang, B. Chen, L. Zhang, J. Huang, F. Chen, Z. Yang, J. Yao and Z. Zhang, *Nanoscale*, 2011, **3**, 1446-1450; (b) X. Yang, X. Zhang, Y. Ma, Y. Huang, Y. Wang and Y. Chen, *J. Mater. Chem.*, 2009, **19**, 2710-2714; (c) W. Chen, P. Yi, Y. Zhang, L. Zhang, Z. Deng and Z. Zhang, *ACS Appl. Mater. Int.*, 2011, **3**, 4085-4091; (d) G. Xie, P. Xi, H. Liu, F. Chen, L. Huang, Y. Shi, F. Hou, Z. Zeng, C. Shao and J. Wang, *J. Mater. Chem.,* 2012, **22**, 1033-1039.

11 W. S. Hummers and R. E. Offeman, *J. Am. Chem. Soc.*, 1958, **80**, 1339-1339.

12 D. R. Dreyer, S. Park, C. W. Bielawski and R. S. Ruoff, *Chem. Soc. Rev.*, 2010, **39**, 228-240.

13 H. Yang, J. Jiang, W. Zhou, L. Lai, L. Xi, Y. Lam, Z. Shen, B. Khezri and T. Yu, *Nanoscale Res. Lett.*, 2011, **6**, 531.

14 A. H. Elsayed, M. S. Mohy Eldin, A. M. Elsyed, A. H. Abo Elaz, E. M. Younes and H. A. Motaweh, *Int. J. Electrochem Sci.*, 2011, **6**, 206-221.

15 (a) L. C. Branquinho, M. S. Carriao, A. S. Costa, N. Zufelato, M. H. Sousa, R. Miotto, R. Ivkov and A. F. Bakuzis, *Sci. Rep.*, 2013, **3**; (b) C. Martinez-Boubeta, K. Simeonidis, A. Makridis, M. Angelakeris, O. Iglesias, P. Guardia, A. Cabot, L. Yedra, S. Estrade, F. Peiro, Z. Saghi, P. A. Midgley, I. Conde-Leboran, D. Serantes and D. Baldomir, *Sci. Rep.*, 2013, **3**; (c) Y. Pineiro-Redondo, M. Banobre-Lopez, I. Pardinas-Blanco, G. Goya, M. A. Lopez-Quintela and J.

New Journal of Chemistry Accepted Manuscript

Rivas, *Nanoscale Res. Lett.*, 2011, **6**, 383; (d) A. Urtizberea, E. Natividad, A. Arizaga, M. Castro and A. Mediano, *J. Phys. Chem. C*, 2010, **114**, 4916-4922; (e) C. Martinez-Boubeta, K. Simeonidis, D. Serantes, I. Conde-Leborán, I. Kazakis, G. Stefanou, L. Peña, R. Galceran, L. Balcells, C. Monty, D. Baldomir, M. Mitrakas and M. Angelakeris, *Adv. Funct. Mater.*, 2012, **22**, 3737-3744.

16 (a) S.-H. Hu, Y.-W. Chen, W.-T. Hung, I. W. Chen and S.-Y. Chen, *Adv. Mater.*, 2012, **24**, 1748-1754; (b) B. J. Hong, O. C. Compton, Z. An, I. Eryazici and S. T. Nguyen, *ACS Nano*, 2011, **6**, 63-73

New Journal of Chemistry Accepted Manuscript

 This journal is © The Royal Society of Chemistry 2012